Cell, Vol. 108, 769–780, March 22, 2002, Copyright ©2002 by Cell Press

Structure of the C3b Binding Site of CR1 (CD35), the Immune Adherence Receptor

Brian O. Smith,[1,4] Rosie L. Mallin,[1,4] Malgorzata Krych-Goldberg,[2] Xuefeng Wang,[2] Richard E. Hauhart,[2] Krystyna Bromek,[1] Dusan Uhrin,[1] John P. Atkinson,[2] and Paul N. Barlow[1,3]

[1]Edinburgh Protein Interaction Centre
Joseph Black Chemistry Building
University of Edinburgh
West Mains Road
Edinburgh EH9 3JR
United Kingdom

[2]Division of Rheumatology
Department of Medicine
Washington University School of Medicine
St. Louis, Missouri 63110

Summary

Complement receptor type 1 (CR1 or CD35) is a multiple modular protein that mediates the immune adherence phenomenon, a fundamental event for destroying microbes and initiating an immunological response. It fulfills this role through binding C3b/C4b-opsonized foreign antigens. The structure of the principal C3b/C4b binding site (residues 901–1095) of CR1 is reported, revealing three complement control protein modules (modules 15–17) in an extended head-to-tail arrangement with flexibility at the 16-17 junction. Structure-guided mutagenesis identified a positively charged surface region on module 15 that is critical for C4b binding. This patch, together with basic side chains of module 16 exposed on the same face of CR1, is required for C3b binding. These studies reveal the initial structural details of one of the first receptor-ligand interactions to be identified in immunobiology.

Introduction

Immune adherence, first described at the beginning of the 20th century, was rediscovered in the 1950s (Nelson, 1953, 1963). It refers to binding of serum-exposed particles to blood cells, which is a fundamental event for initiating and promoting the destruction of microbes and for an immunological response. This interaction is dependent on the coating of the antigenic particle with complement and recognition by a factor on the erythrocyte surface—the immune adherence receptor.

Activation of complement leads to deposition of C4b and C3b on a target. Complement receptor type 1 (CR1, CD35) (reviewed Krych-Goldberg and Atkinson, 2001) binds to these immobilized ligands and is the immune adherence receptor. In addition, CR1 regulates further complement activation by accelerating the decay of key proteolytic complexes, the C3 and C5 convertases, and by serving as a cofactor for limited cleavage of C4b and C3b. The resulting bound C3 fragments are ligands for other complement receptors. CR1 is expressed by most blood cells and its function varies depending upon cell type. CR1 on erythrocytes binds and processes immune complexes and transfers them to the liver and spleen. On granulocytes and monocytes/macrophages, CR1 mediates attachment and ingestion of complement-coated targets. On B lymphocytes and follicular-dendritic cells, CR1 facilitates localization of complement-coated antigens to immunocompetent cells. Of recent interest is the interaction between the C3b binding site of CR1 and a major adhesin of *Plasmodium falciparum*-infected erythrocytes (Rowe et al., 1997, 2000); this interaction leads to rosetting between infected and uninfected erythrocytes, a phenomenon correlated with severe malaria.

The N-terminal extracellular portion of CR1 is composed of 30 repeats of 59–72 amino acids (aa) (Klickstein et al., 1987, 1988; Hourcade et al., 1988). These fold into modules, linked by nonconserved sequences of four to eight aa. Homologous modules are prevalent among the regulators of complement activation (RCA) family (Liszewski and Atkinson, 1998) and are known as complement control protein modules (CCPs) (also known as sushi domains and short consensus repeats) (Reid and Day, 1988). Apart from four consensus Cys and a conserved Trp, significant sequence diversity is present among CCP sequences, and insertions and deletions are commonplace. Three-dimensional structures have been solved of ~12 CCPs (Kirkitadze and Barlow, 2001; Szakonyi et al., 2001) but not of any of the CR1 CCPs. Despite a broadly similar structural framework, there are variations in loops and turns. These contribute to significant and functionally critical differences in the arrangement of adjacent CCPs.

CR1 has two functionally distinct sites (Klickstein et al., 1988; Krych et al., 1991). Site 1 (CCPs 1–3) binds mainly C4b and has convertase decay accelerating activity (DAA), while two nearly identical copies of site 2 (localized to modules 8–10 and 15–17; Figure 1) bind C3b and C4b and have factor I-cofactor activity (CA) with respect to both proteins (Krych et al., 1991, 1994, 1998; Krych-Goldberg et al., 1999). In prior homologous substitution-mutagenesis studies of sites 1 and 2, some single aa substitutions reduced binding of one or both ligands (Krych et al., 1991, 1994, 1998; Krych-Goldberg et al., 1999). In some cases reciprocal changes in sites 1 and 2 led to a loss of function at one site and to a gain of the same function at the other site. Although key amino acids for DAA and CA were identified, a complex picture emerged. Moreover, the results of homologous substitution mutagenesis did not identify potential contact points in the first module of either site and offered no explanation as to how these CCPs participate in binding. Lack of a 3D structure of CR1, or of any mammalian C3b/C4b binding protein, has thus hampered further understanding.

The 3D structure of an individual CCP is difficult to model with confidence due to sequence variation, and the orientation and flexibility of neighboring CCPs with

[3]Correspondence: barlow@chem.ed.ac.uk
[4]These authors contributed equally to this work.

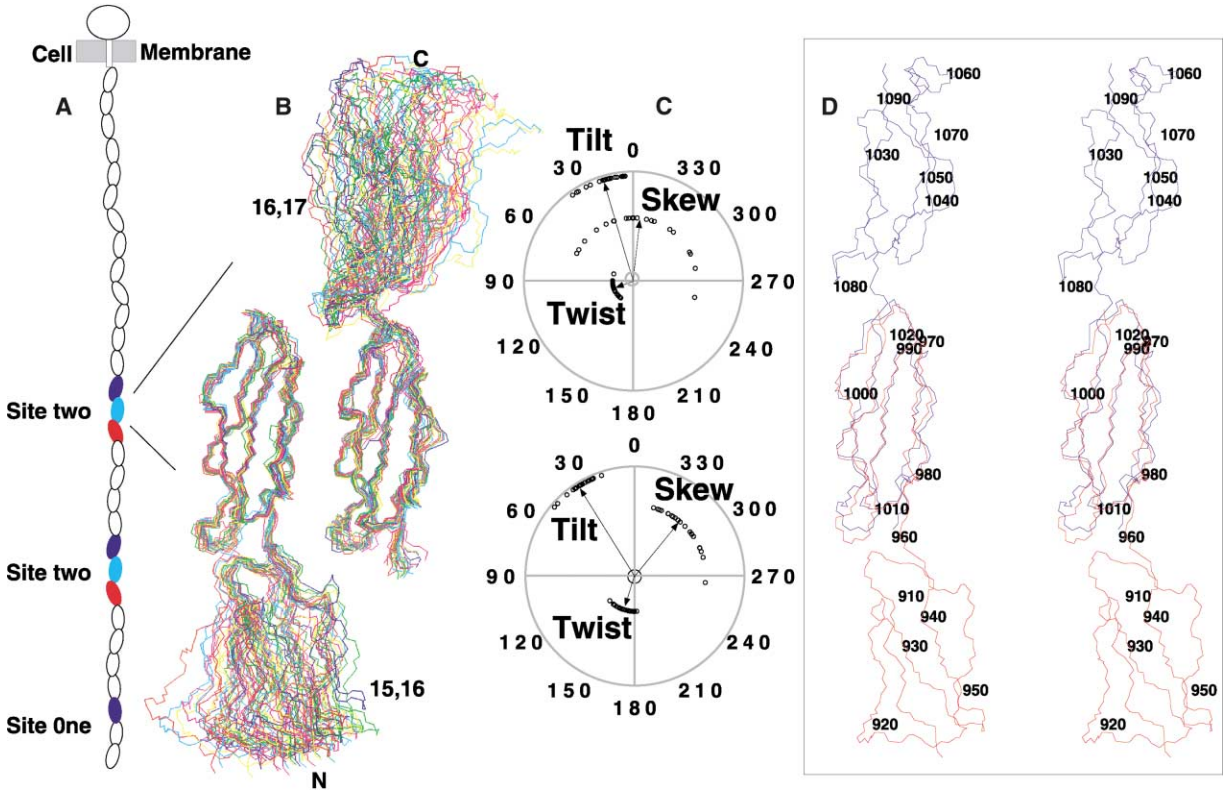

Figure 1. NMR-Derived Structures of Site 2 from CR1

(A) Location of CCPs 8 and 15 (red), CCPs 9 and 16 (cyan), and CCPs 3, 10, and 17 (blue) in CR1.

(B) Backbone overlays of NMR-derived structures. In each case 24 structures are overlaid on Cα atoms of CCP 16 (mean structure).

(C) Distribution of tilt, twist, and skew angles among the two ensembles of structures. Arrows show mean angles.

(D) The structure (backbone; stereopair) closest to the mean of the CR1∼15,16 structures (red) overlaid on module 16 (Cα's) of the equivalent structure from the CR1∼16,17 ensemble (blue).

respect to one another vary considerably and are unpredictable. Therefore, to understand the structural basis of immune adherence and of complement control, it is necessary to solve experimentally the 3D structures of the triple-CCP functional sites. We now report the solution structure of CCPs 15, 16, and 17 of human CR1 (CR1∼15–17, site 2). The structure has allowed rationalization of an extensive body of mutagenesis and design of new mutagenesis experiments. In the absence of direct structural studies of the C3b/CR1 interaction, these data provide the most detailed understanding so far of the molecular basis of immune adherence, some 100 years after its discovery.

Results

Nuclear magnetic resonance (NMR) data collected on CR1∼15–17 permitted assignment of >90% of backbone ^{15}N, ^{13}Cα, ^{13}C(O), and ^{13}Cβ resonances. The sensitivity of side chain experiments collected on samples of CR1∼15–17 was, however, too poor for complete assignment. To circumvent this, the two overlapping module pairs (CR1∼15,16 and CR1∼16,17) were investigated. These proteins were fully assigned and yielded NOESY spectra suitable for structure determination.

Figure 1 shows backbone overlays, on CCP 16, of the ensembles of structures calculated for these overlapping module pairs (structural statistics, Table 1). The root mean square deviation (rmsd) of the Cα atoms from the respective mean structures is plotted for each pair in Figure 2 along with the number of nuclear Overhauser effects (NOEs) per residue. Values of rmsd were based on overlaying each module in turn and excluding disordered residues (i.e., with low ^{1}H,^{15}N-NOE). Overall rmsd values (Table 1) indicate that individual modules are quite well defined by the data.

There are no significant differences in CCP 15 chemical shifts (δs) when the 15,16 pair is compared to CR1∼15–17 (data not shown). Context-dependent differences in the δs of CCP 17 (i.e., in CR1∼15–17 versus in CR1∼16,17) arise only from the nonidentical C termini of the two fragments; no changes are attributable to the presence or absence of CCP 15. Thus, CCPs within site 2 are arranged such that CCPs 15 and 17 are not in direct contact, consistent with previous studies (Kirkitadze et al., 1999a, 1999b). Comparison of the δs of module 16 in CR1∼15,16 ($^{(15)}$16), in CR1∼16,17, (16$^{(17)}$), and in CR1∼15–17 ($^{(15)}$16$^{(17)}$) shows that CCP 16 exhibits context-dependent changes in δs near (in space) its N and C termini, but not elsewhere. The structures of modules $^{(15)}$16 and 16$^{(17)}$ are not significantly different (Figures 1 and 2); the rmsd is 0.58 Å (for the Cα overlay), excluding disordered residues. These observations all imply that

Table 1. Structural Statistics for the 24 Lowest Energy Structures

	CR1∼15,16	CR1∼16,17	
Total unambiguous NOEs	2869	2331	
Total ambiguous NOEs	455	226	
Hydrogen bonds	29	25	
For unambiguous NOEs			
Sequential	664	564	
Short-range ($2 \leq \|i-j\| \leq 4$)	194	146	
Long-range ($\|i-j\| > 4$)	786	563	
Intermodule	13	4	
Intralinker	74	69	
From 17 to 16,17 linker	–	29	
From 16 to 16,17 linker	–	39	
From 16 to 15,16 linker	46	–	
From 15 to 15,16 linker	48	–	
For ambiguous NOEs			
Sequential	148	69	
Short range ($2 \leq \|i-j\| \leq 4$)	36	25	
Long range ($\|i-j\| > 4$)	225	93	
Intermodule ambiguous NOEs	1	0	
Intralinker ambiguous NOEs	17	3	
From 17 to 16,17 linker	–	1	
From 16 to 16,17 linker	–	8	
From 16 to 15,16 linker	12	–	
From 15 to 15,16 linker	28	–	
Total (all structures) NOE violations > 0.5	33	44	
Rmsds for ensemble of 24[a] ± SD			
NOE (Å)	0.0329 ± 0.0026	0.0370 ± 0.0034	
Bond lengths (Å)	0.0022 ± 0.0001	0.0021 ± 0.0001	
Bond angles (°)	0.3936 ± 0.0173	0.3734 ± 0.0233	
Rmsds for representative structure[a]			
NOE (Å)	0.0034	0.0037	
Bond lengths (Å)	0.0022	0.0020	
Bond angles (°)	0.3933	0.3613	
Percent of residues in regions of Ramachandran plot			
Most favored	67.9	60.0	
Additionally allowed	24.8	28.2	
Generously allowed	5.5	5.5	
Root mean square deviations[b]	15	16	17
Backbone atoms Cα, N, CO	0.677	0.734	1.103
Cα only	0.687	0.759	1.148

[a] Representative structure is closest to the mean of the appropriate ensemble of 24 structures.
[b] From Cys1 to Cys4, excluding residues (1) with heteronuclear NOE values less than one SD lower than mean and (2) for which relaxation data were unavailable. Average of $^{(15)}16$ and $16^{(17)}$ values shown for CCP 16.

the structure of CR1∼15–17 can be reconstructed by superimposing the structures of $^{(15)}16$ and $16^{(17)}$ (see Figure 1). To create the model, structures closest to the mean of each of the two ensembles of calculated module-pair structures were used as input for the program Modeller (Sali and Blundell, 1993; see Experimental Procedures).

Each of the three CCPs of site 2 has a structure consisting of extended regions and antiparallel β strands, connected by loops. Extended regions classified (Promotif [Hutchinson and Thornton, 1996]) as β strands in >50% of the ensemble are shown in Figure 3. The extended regions (whether or not categorized as β strands) in each module were denoted A–H (only β strands are labeled in Figure 3). Each module has an elongated shape, with a long axis running between the N and C termini. The strands are, for the most part, aligned with the long axis, and connecting loops are close to the intermodular interfaces. The disulphides, Cys(I)-Cys(III) and Cys(II)-Cys(IV), are well spaced, and the consensus Trp and other conserved residues contribute to a hydrophobic core within each module.

Residues (Figure 2) with high ^{15}N T_1 values, high T_2s, and negative $^1H,^{15}N$ NOEs occur at the N termini of both module pairs, indicating that these regions (before Cys(I) of the first module) are highly mobile on the ps–ns timescale. The residues at the N terminus of CCP 16 become significantly less mobile upon attachment of CCP 15. Residues at the C terminus of CCP $^{(15)}16$ and of CCP 17 have less ps–ns motion. In general, dips in the plot of $^1H,^{15}N$ NOEs are accompanied by longer T_1s and T_2s and correspond to loops consistent with the flexibility of these regions. Some residues were deemed to be undergoing slower scale (μs–ms) motion (on the basis of application of the criteria of Barbato et al., 1992; Figure 2).

The CCPs are assembled in head-to-tail fashion (Figure 3). The mutual orientation of CCPs 15 and 16 is determined experimentally by a network of 13 unambig-

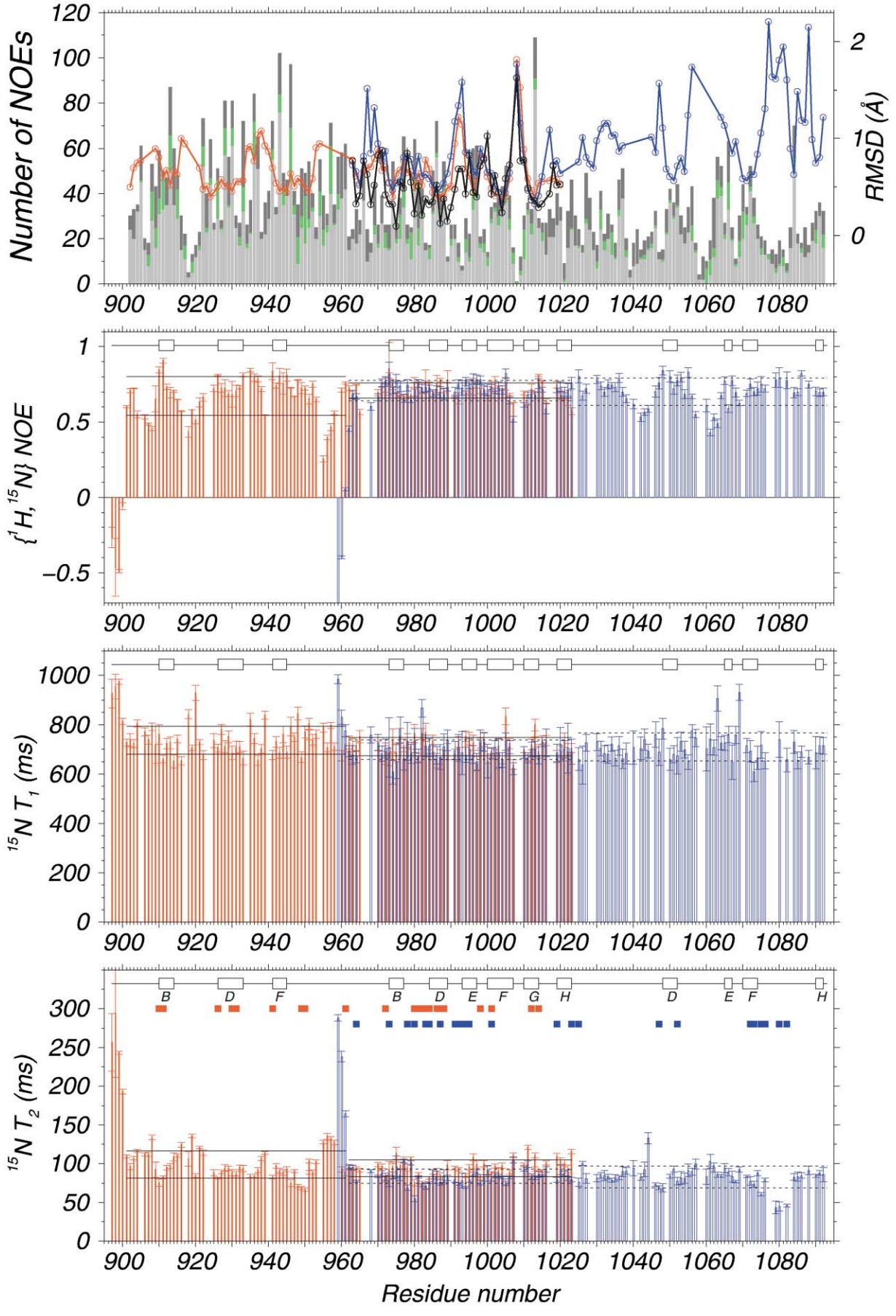
Number of NOEs
RMSD (Å)
{1H, 15N} NOE
15N T1 (ms)
15N T2 (ms)
Residue number
B D F B D E F G H D E F H

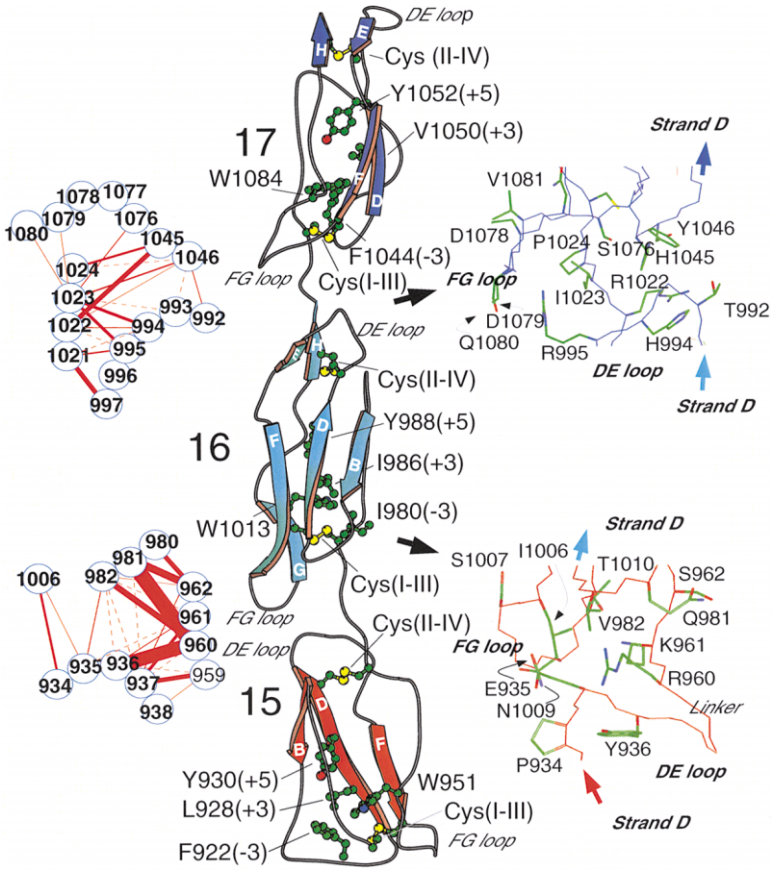

Figure 3. Modules and Intermodular Junctions of Site 2

In the center is shown a representation (Kraulis, 1991) of the CR1∼15–17; same view as in Figure 1. Eight side chains are shown in each module; parenthetical number (−3, +3, +5) indicates position relative to the conserved Gly at the N terminus of strand D. On the left, schematics illustrate occurrence (red lines) of intermodular and module-linker NOEs within the 15,16 (bottom) and 16,17 junctions. Dotted lines indicate one NOE, solid lines indicate more than one; thickness of line is proportional to number of NOEs.

On the right are shown details of junctions (same view as on left) with backbone trace in red (15,16) or blue (16,17) and side chains atoms colored green, C; blue, N; red, O; and yellow, S.

uously assigned NOEs between the bodies of the modules and a total of 134 NOEs (94 of them unambiguously assigned) between the linker and the modules (Figure 3, Table 1). Analysis of 55 ^{1}H-^{15}N residual dipolar couplings measured for CR1∼15,16 in hexanol/cetylpyridinium bromide medium (data not shown) are compatible with CCPs 15 and 16 having the same alignment tensor, which is evidence in support of a defined association between modules. Moreover, the dipolar couplings are also consistent with the relative orientations seen in the ensemble of structures (Figure 3) derived from NOEs and J couplings. In the 15-16 junction, the carbonyl oxygen of linker residue Lys961 has an inferred H bond to the NH of Val982 (in the CD loop of CCP 16), and an H bond from the NH of Lys961 to the backbone carbonyl oxygen of Glu935 (in CCP 15) was inferred. Side chains of linker residues Arg960 and Lys961 are in van der Waals contact with Tyr936 and Tyr937, respectively, of CCP 15. The side chains of both these linker residues also contact the CH_3 protons of Val982 (module 16). Strand F of CCP 16 approaches the DE loop (i.e., loop between strands D and E) of CCP 15, and a CH_3 of Leu1006 contacts Glu935.

The 16-17 junction is less well defined by distance restraints between modules (Figure 3, Table 1). The preferred orientation that emerges from the calculation is determined by only 4 intermodular NOEs and by 68 unambiguous and 9 ambiguous NOEs between the linker and the two modules. This junction is more open with few hydrophobic contacts. The side chain of Arg995 in strand E of CCP 16 could contact residues in the FG loop of CCP 17, but the latter is flexible. The first two residues of the 16-17 linker (aa 1021 and 1022) are closely associated with CCP 16, but the side chains of the next two residues do not form part of a larger hydrophobic pocket as seen in other junctions. Given the relatively small number of NOEs defining the 16-17 junction, the poor definition (Figure 1) in intermodular orientation may reflect flexibility between CCPs 16 and 17. The ^{1}H-^{15}N NOEs of amides in the 16-17 linker are

Figure 2. Experimental NMR-Derived Data

The top graph summarizes the data used for the structure calculations and the precision of the calculated structures. The number of distance restraints per residue are shown (bars, left-hand scale): sequential (residue i − residue i+1) in dark gray, short range (i−(i+(<5)) in green, and long range (i−(i+(>4)) in light gray. Root-mean-square deviations (rmsds) of the Cα coordinates of well-ordered residues in each module from its mean structure are plotted (o, lines, right-hand scale; 15,16 [red] and 16,17 [blue]) as is the Cα rmsd between the mean structures of $^{(15)}16$ and $16^{(17)}$ (black).

Lower three graphs: ^{15}N T_1, heteronuclear NOEs, and ^{15}N T_2 for 15,16 (red) and 16,17 (blue) versus residue number. Mean ± SD is shown for each module by a horizontal black line (dotted for 16,17). Secondary structure is indicated. In the T_2 panel, red (15,16) and blue (16,17) squares indicate residues mobile on μs–ms timescale (based on ^{15}N T_1 and T_2).

similar to those for the 15-16 linker. They do not indicate flexibility on the ps–ns timescale, and only Ile1023 is flexible on the μs–ms timescale but CCP 16-CCP 17 flexibility could still be in the order of 10^8 s^{-1}.

Intermodular orientations are characterized by tilt, twist, and skew (Barlow et al., 1993; Bork et al., 1996). In both junctions, the tilt angles within the ensemble of calculated structures are ~20°–30°; the tilt of CCP 17 compared to CCP 15 (in the reconstruction) is 39°. The twist angle at the 15,16 junction is close to 180°; the twist at the 16,17 junction is closer to 90°, and the twist of CCP 17 compared to CCP 15 (in the reconstruction) is ~280°. Consequently, the three modules trace a gentle curve (Figure 3), and equivalent regions of the three modules such as the hypervariable loops (Wiles et al., 1997) face in different directions. Skew angles are less well defined, especially at the 16,17 junction. The elongated shape of site 2 results in a large solvent-exposed surface area with potential for extensive contacts with binding partners.

Since despite extensive mutagenesis experiments no strong candidates for key contact points had previously been identified in CCP 15, the NMR-derived structure of CR1 site 2 was utilized to perform a search for critical residues in this module. Based on previous studies (Krych et al., 1994, 1998), residues in CCP 15 lying on the same face of the triple module as functionally critical Asn1009 and Lys1016 of CCP 16 were considered candidates. Among these, residues with basic side chains were selected for mutagenesis because it has been shown that acidic residues of C3b are involved in binding CR1 (Oran and Isenman, 1999). A patch of basic side chains in module 15—Lys912 and Lys914 in strand B and Arg933 at the end of strand D—lie on this "front" face (Figure 4). Changing all three to Glu abrogated C4b binding and significantly reduced C3b binding (Figure 5). When these three mutations of module 15 were combined with K1016E in CCP 16, C3b binding was further reduced, even at low salt. Another surface Lys (964) on CCP 16 was observed to lie roughly equidistant from Asn1009 and Lys1016 and on the left-hand side of the front face as viewed in Figure 4. Charge reversal here (K964E) enhanced the effects of the combined mutations K912E, K914E, and R933E in CCP 15 to a similar extent as the K1016E mutation. When all five basic side chains (Lys912, Lys914, and Arg933 in module 15 and Lys964 and Lys1016 in module 16) were mutated to Glu, C3b binding was reduced to 35% (low-salt) or <10% (100 mM salt) (Figure 5). An assay for cofactor activity for C3b showed that in each case cofactor activity paralleled that of ligand binding.

Discussion

An understanding of the mechanism of interaction between CR1, which is the immune adherence receptor, and C3 is important since it is the basis of some of the most ancient and fundamental of immunological processes. Immune adherence allows C3 to act as nature's adjuvant for the humoral immune response and to carry out its roles in facilitating phagocytosis and in the processing of immune complexes. Binding of CR1 to C3b/C4b is also critical to the complement system.

Structure of Site 2

The structure of functional site 2 (CCPs 15, 16, and 17) of CR1, which is the main locus of C3b binding, was determined by combining solution structures of the overlapping CCP pairs, CR1~15,16 and 16,17, and validated by a chemical shift comparison with CR1~15–17. In determining the structure of CR1~15–17, the structure of CR1~8–10 (identical bar three residues) has also been effectively solved, as has the structure of module 3 (Figure 1). Further, because CCPs 1 and 2 are 61% identical to CCPs 15 and 16, respectively, the current results provide a reliable basis for the modeling by homology of these CCPs of site 1.

A network of 107 long-range NOEs involving five residues in the DE loop of module 15, all residues of the linker, and four residues in two loops of module 16 provide an experimentally derived definition of the relative orientations of modules 15 and 16 that is supported by residual dipolar couplings. Therefore, this junction must be relatively rigid. Fewer NOEs provide experimental validation of the 16-17 orientation, and in agreement with previous work (Kirkitadze et al., 1999a, 1999b), this junction is likely to be less tight than the 15-16 one. Residues within the 16-17 linking sequence do not have significantly different relaxation properties to the 15-16 linker. Nevertheless, 10^{-8} s motion of CCP 16 relative to CCP 17 cannot be excluded (Copie et al., 1998) and would be consistent with the small intermodular interface and the lack of definition of the skew angle among the ensembles of NMR-derived structures. Evidence of flexibility between modules has been found in studies of MCP (Casasnovas et al., 1999), factor H (Barlow et al., 1993), and VCP (in solution) (Henderson et al., 2001) but not in the crystal structures of VCP (Murthy et al., 2001) or β-2-glycoprotein I (B2GPI) (Bouma et al., 1999; Schwarzenbacher et al., 1999).

Comparison with Structures of Other CCPs

The structure of site 2 is elongated with an axial ratio of ~5:1, consistent with hydrodynamic studies (Kirkitadze et al., 1999c). Anisotropic tumbling might explain the broad NMR resonances that precluded direct determination of the CR1~15–17 structure. The CCPs each have a broadly similar structure to their counterparts in VCP (modules 1–3) and MCP (modules 1 and 2). The closeness (rmsd of 1.1 Å over backbone atoms of 58 residues) between the structures of CCP 16 of CR1 and CCP 2 of MCP (22 sequence identities, 8 conservative replacements) is surprising, since there are several nonconserved prolines toward the N terminus and these two CCPs have no known functional similarities. On the other hand, a comparison of CR1's CCP 16 and CCP 2 of VCP (22 identities, 7 conservative replacements) gives a relatively poor rmsd of 2.0 Å over 43 residues. The best rmsd that can be achieved between MCP~1 and CR1~15 (15 identities, 4 conservative replacements) is 2.0 Å over 27 residues. These comparisons illustrate the importance of experimental structure determination of CCPs despite the availability of homologous structures. However, the most important aspect of the current work lies in the elucidation of intermodular orientations, since these cannot be predicted with reliability by homology.

A range of configurations of neighboring CCPs have

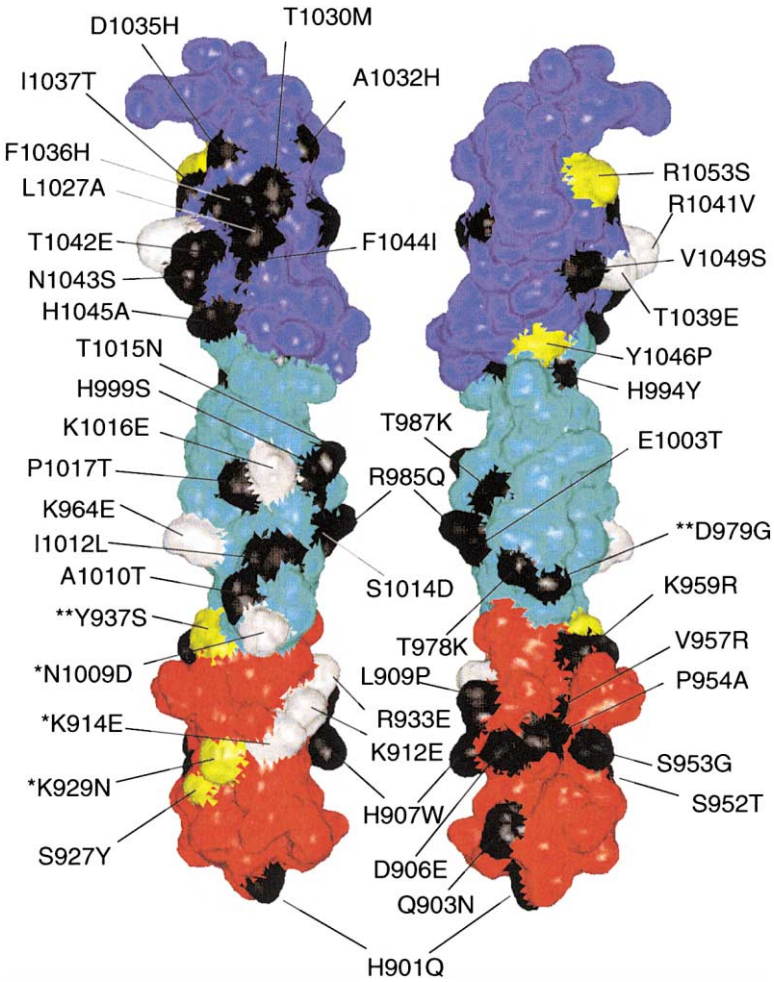

Figure 4. Mutations Mapped onto Surface of Site 2

Left: surface of CR1∼15–17 using color scheme (red, 15; cyan, 16; blue, 17), except where mutagenesis yielded no significant loss of C3b (iC3) binding or C4b binding (black), some loss of C3b (iC3) binding (aa 937, 1053) or C4b binding (aa 927, 929, 1046) (yellow), or major loss of C3b and/or C4b binding (white). Single asterisk indicates residues that, when incorporated at their equivalent positions in site 1 (i.e., D109N, N29K, and T14K), caused gain of C3b binding. Double asterisk indicates two residues (Y27S/G79D) that confer C3b binding activity when simultaneously inserted at their equivalent positions in site 1.

Right: same features but rotated (about vertical axis) by 180°.

been observed in the 3D structures solved to date. In VCP, modules 3 and 4 have a relatively large tilt angle (Wiles et al., 1997; Murthy et al., 2001), as do MCP modules 1 and 2 (Casasnovas et al., 1999), while CCPs 1 and 2 of CR2 exhibit a unique side-to-side packing (Szakonyi et al., 2001). The most common arrangement is head-to-tail, as seen in B2GPI (Bouma et al., 1999; Schwarzenbacher et al., 1999), factor H (modules 15 and 16; Barlow et al., 1993), VCP modules 1 and 2 (Murthy et al., 2001), and now in CR1. It is noteworthy, however, that angles of tilt, twist, and skew are different in each case. For example, the MCP∼1, 2 junction is more kinked (tilt equals 75°) than the 15,16 one, and there is little in common between the 1,2 junction of VCP and the 15,16 junction of CR1, or between the 2,3 junction of VCP and the 16,17 junction of CR1, resulting in different intermodular orientations.

Implications for the Structure of Site 1 (CCPs 1–3)

Although in general CCPs exhibit high sequence diversity, the CCPs of site 2 of CR1 are similar to the CCPs (1–3) of its site 1. Comparison of CCP 15 with CCP 1 (31 identities, 6 conservative replacements), CCP 16 with CCP 2 (42 identities, 4 conservative replacements), and CCP 3 with CCP 17 (two replacements) indicates that the three individual modules of site 1, for which no structures have been determined, will be highly similar in structure to those of site 2 (with the exception of some flexible loops and localized changes in strands B and C and the GH bulge associated with nonconserved Gly and Pro residues). What about the intermodular junctions of site 1? Several of the amino acids important in the interface between CCPs 15 and 16 are conserved, or conservatively replaced, in site 1. However, Tyr937 is replaced by a Ser, and Glu935 is replaced by a Gly. Thus, the 1,2 interface is probably different from the 15,16 interface, in agreement with the different thermodynamic unfolding profiles of site 1 versus site 2 (Kirkitadze et al., 1999a; Clark et al., 1996). It is possible that the looser 16,17 junction resembles that between CCPs 2 and 3, since the DE regions of CCPs 16 and 2 are similar and the linker sequences and the sequences of the FG and CD regions of CCPs 17 and 3 are identical.

Mutagenesis and Functional Implications

The availability of a 3D structure of the complete, functional site 2 of CR1 allows rationalization of extensive mutagenesis experiments. Previously, homology-based models have been used to explain mutagenesis data (e.g., Kuttner-Kondo et al., 2001; Liszewski et al., 2000; Villoutreix et al., 1998), since experimentally determined structures were unavailable. The cocrystallization of

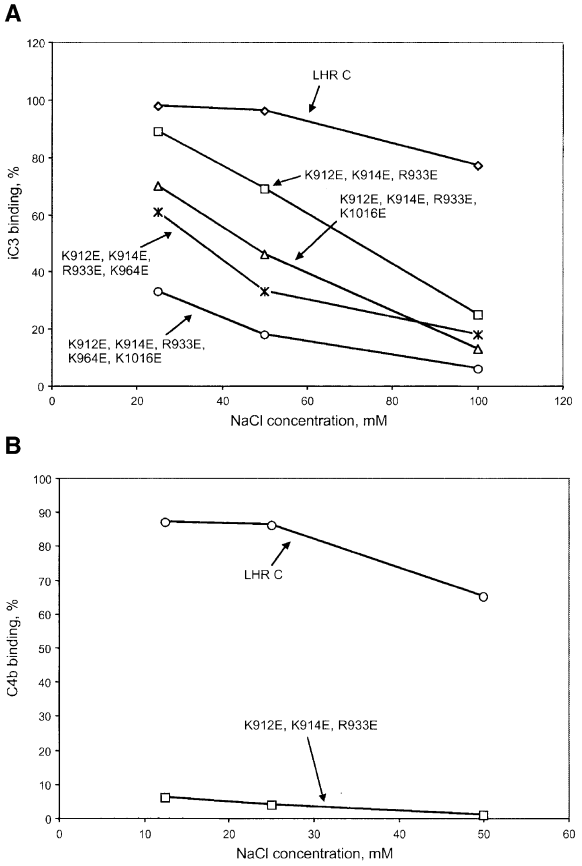

Figure 5. Ligand Binding by Charge-Reverse Mutants in Site 2

(A) iC3-Sepharose

(B) C4b-Sepharose

One representative measurement of two-to-four is shown by each data point. In the case of C4b binding, mutants had binding values of ≤6% compared to the parent fragment. Results are expressed as a percentage of CR1 derivative bound to iC3-S or C4b-S of that initially offered to the Sepharose.

CCPs 1 and 2 of CR2 with C3d revealed details of that specific interaction, but there are no reports of cocrystallization of RCA proteins with the less experimentally tractable C3b/C4b fragments. Attempts to examine CR1 site 2-C3b interactions in the NMR tube by chemical shift mapping proved unsuccessful (data not shown), presumably due to the large size (180 kDa) and probable dimeric nature of C3b. Experiments using peptides that are representative of C3b also failed (data not shown), probably due to low affinity. Therefore, the substantial body of mutagenesis data for CR1 amassed over the last ten years, when reconsidered in the light of the current structure, provides the best insight yet into an interaction between any member of the RCA family and C3b/C4b.

Figure 4 summarizes the mutagenesis data obtained so far. Not highlighted in Figure 4 is a triple mutation that gave some loss of C3b binding but where the side chains (944, 947, and 949) are dispersed on the surface; drastic mutations in module 17 involving many residues (Krych et al., 1998) are also not shown. The majority of reported mutations of CR1 site 2 did not have a negative effect on its biological activity (Figure 4). Some of the substitutions were conservative (Q903N, D906E, and I1012L), while others were not (e.g., P954A, T987K, and V1049S). This observation supports the notion that the CCP consensus residues provide a structural framework that is very tolerant of amino acid substitutions elsewhere in the sequence. Therefore, mutations of nonconsensus amino acids that have side chains known to be exposed at the surface and not involved in intramolecular module-module contacts are unlikely to significantly disturb the structure of the protein. The implication is that where such mutations abrogate function, they are likely to be in direct contact with binding partners.

In the case of module 15, one face ("front" in Figure 4) carries several side chains that contribute to C3b binding and (especially) C4b binding, while no such residues have so far been identified on the "back" face. Module 16 is oriented in a relatively well-defined manner with respect to module 15, and N1009, which resides in the flexible FG loop of module 16, lies on the same front face as CCP 15 residues that are critical for binding. It is interesting that the substitution of several of these amino acids (N1009, K914, and K929) for their equivalents in site 1 causes site 1 to gain significantly in its ability to bind C3b (Krych et al., 1998; Krych-Goldberg et al., 1999). Other CCP 16 residues implicated by mutagenesis also lie on this front face, while no such residues have so far been detected on the back face (Figure 4). Furthermore, the back face of module 16 carries the glycosylation site, N987 (mutated to Thr in the NMR sample, hence T987 in Figure 4); glycosylation does not influence C3b or C4b binding. Therefore, it appears probable that the front face of site 2 contacts C3b and C4b. The most dramatic results were obtained where positively charged or neutral side chains were replaced with negatively charged ones, indicating that positive charge is favorable to binding. An interaction with a dominant electrostatic component has been indicated previously by its salt dependency (Krych et al., 1994, 1998; Krych-Goldberg et al., 1999), because positively charged regions of other RCA proteins have been implicated in binding to C3b/C4b (Kuttner-Kondo et al., 1996; Blom et al., 2000) and due to the involvement of negatively charged residues at the N terminus of C3b in interactions with RCA proteins (Oran and Isenman, 1999).

Several nonconservative substitutions on the front face, however, have no effect on binding, implying that the interaction probably does not involve a contiguous set of residues forming an intimate interface. This is consistent with the dispersed (over several neighboring modules) nature of the CR1-C3b/C4b interaction and its low-to-medium affinity, i.e., 0.1–0.5 μM for the CR1/C4b interaction (Reilly and Mold, 1997) and 0.6 μM and 0.03 μM for the C3b monomer and dimer, respectively (Weisman et al., 1990; Wong and Farrell, 1991). It is also comparable with the CR2-C3d interface revealed by crystallography (Szakonyi et al., 2001) that shows a significant involvement of the peptide backbone in addition to a few side chain contacts involving positively charged residues. Arg84 of CR2 occupies an anionic hole in C3d, and Lys100 of CR2 participates in H_2O-mediated H bonds with C3d. Module 2 of CR2 and CCP 15 of CR1 share 19 identical or conservatively replaced residues and there are small insertions and deletions. The two

CCPs overlay reasonably well (1.7 Å, using the Cα of 22 residues). Equivalent residues to CR2's Arg84 and Lys100 are Lys914 and Arg933, both of which are critical to the CR1-C3b interaction. Whether CR1 interacts with the C3d portion of C3b as well as its N terminus is debatable (Oran and Isenman, 1999; Cole et al., 1985).

Several residues on CCP 17 were also shown to be critical for C3b/C4b binding. These appear not to lie on the same face of site 2 as the functionally-critical residues of CCPs 15 and 16, according to the preferred orientation derived from NMR restraints (Figure 4). Given the likely loose nature of the 16,17 junction, module 17 could swivel relative to module 16 in order to align its binding face with that of 15,16. In support of this hypothesis, changes of residues at the 16,17 interface have little or no effect on C3b binding—for example, mutating the almost completely buried I1023 to Pro does not lower affinity for either protein, while mutation of substantially buried Y1046 to Pro affects only C4b binding (Krych et al., 1998); it is unlikely that any functionally critical preformed 16,17 orientation would survive these substitutions, but a looser junction would be more tolerant to substitutions provided they did not induce a different preferred conformation. On the other hand, these two substitutions (I1023P and Y1046P) each have a dramatic effect on site 2's activity as a cofactor for factor I-catalyzed proteolysis of C3b/C4b (Krych et al., 1998). Therefore, a specific kind of flexibility at the 16,17 junction appears to be critical for this particular aspect of site 2's biological function. The mutation Y937S, close to the 15,16 junction, also reduces cofactor activity (Krych et al., 1994).

Unlike in previous work, these structure-guided mutagenesis experiments involved changes of residues that are *conserved* between sites 1 and 2. That residues common to both sites are important is unsurprising, since the activities of sites 1 and 2 overlap. Each site interacts with C3b and/or C4b and has both DAA and CA, albeit to very different degrees. It is likely that the conserved amino acids identified here as functionally important in site 2 are also critical in site 1. Although intermodular junctions and hence module-module orientations are probably not conserved between CCPs 15/16 (in site 2) and CCPs 1/2 (in site 1), mutations causing gain of function in site 1 (Krych et al., 1994, 1998; Subramanian et al., 1996) may be interpreted cautiously in the light of the site 2 structure. An example of note is D109N (Krych et al., 1994, 1998). Asn1009, a homolog of D109 in site 2, has no structural role, and if the same is true of D109, it implies C3b binding is enhanced by removing a negative charge or by adding the H bonding capabilities of an Asn. Another gain of function example is N29K. The equivalent site 2 residue is Lys929, and the reverse mutation (K929N) causes only a small loss of C4b binding in site 2. Lys929 is located on the front face (down and to the left of Lys914 in Figure 4). The addition of a positive charge in this region of site 1 might enhance C3b binding, while on the other hand, the removal of a positive charge from the front face of site 2 may not be so important due to compensation by other basic side chains. A striking gain of function arises from the double substitution of S37Y in CCP 1 and G79D in CCP 2 (Subramanian et al., 1996). When made individually these changes have only negligible effects, but together they confer good C3b binding activity on site 1. The equivalent residues in functional site 2 are Tyr937, which contacts the linker residue Lys961, and Asp979, which is also close to the 15,16 junction but on the other face to Tyr937. Indeed, Asp979 is on the back face of module 15, well away from amino acids identified as important in C3b binding by mutagenesis of site 2. The difficulty of rationalizing this important observation emphasizes the need for structure determination of site 1.

Conclusions

This work provides the structural details of the much-studied phenomenon of immune adherence first described more than 100 years ago. It also provides the 3D structure of a functional site from a mammalian regulator of complement activation. It allows rationalization of extensive mutagenesis and functional data in the light of a 3D structure. With the structure of site 2 in hand, it will now be possible to pursue more mutagenesis aimed at fine-mapping of the binding face, further dissection of the C3b and C4b binding and cofactor activities, and definition of the functional roles played by intra- and intermodular flexibility. As a byproduct of this work, a rational design of more selective inhibitors of complement is possible. For example, a protein that binds C3b and inactivates alternative convertases but with no ability to bind C4b and to inactivate classical convertases could be produced based on the mutagenesis of positively charged CCP 15 residues. Since site 2 has recently been shown to bind the *P. falciparum* protein PfEMP1 (Rowe et al., 2000), the design of selective inhibitors of this interaction, with therapeutic potential in malaria, might also be feasible.

Experimental Procedures

Expression of Protein for NMR

The three fragments of CR1—CR1∼15–17 (modules 15–17, aa 901–1095 of the mature CR1), CR1∼15,16 (modules 15 and 16, aa 901–1024), and CR1∼16,17 (modules 16 and 17, aa 961–1092)—were expressed as described previously (Kirkitadze et al., 1999a). The sequence of each sample was preceded by EAEA—a remnant of the signal peptide of the *Pichia pastoris* α factor. N glycosylation sites were removed (module 15 mutation N918T, module 16 mutation N987T).

For preparation of ^{15}N-labeled sample, yeast was grown in modified medium containing 0.34% yeast nitrogen base (YNB) without aa and without $(NH_4)_2SO_4$, supplemented with 1% $(^{15}NH_4)_2SO_4$. For double-labeled samples, yeast was grown in modified medium containing 0.34% YNB without aa and without $(NH_4)_2SO_4$, supplemented with 1% $(^{15}NH_4)_2SO_4$ and 0.25% ^{13}C-glycerol in the preculture or 0.25% ^{13}C-methanol during the expression phase. For the (80%) ^{2}H-labeled sample, yeast was grown in glycerol-containing minimal medium in which H_2O was replaced with increasing concentrations (from 40% to 80%) of ^2H_2O.

A 0.6 mM (25 mM phosphate, 150 mM NaCl [pH 6.0]) sample of ^{2}H (80%), ^{13}C,^{15}N-labeled CR1∼15–17 yielded interpretable TROSY-type spectra and was used to obtain backbone and Cβ assignments. Due to side chain deuteration, this sample was unsuitable for full assignment or structure calculation based on ^{1}H,^{1}H NOEs. Therefore, ^{13}C,^{15}N-labeled samples of overlapping module pairs CR1∼15,16 and CR1∼16,17 (1 mM, in 0.6 ml 20 mM potassium phosphate buffer, 20 mM NaCl [pH 6.0]) were used. Relaxation studies used ^{15}N-labeled samples of CR1∼15,16 and CR1∼16,17 in the same buffer and at the same concentration.

Data Collection/Processing

For the ^{2}H (80%), ^{13}C,^{15}N-sample TROSY-versions (Salzmann et al., 1999) (at 37°C) of the HN(CA)CO and HNCACB experiments were

collected at 800 MHz, and HNCO, HN(CO)CACB, HNCOCA, and HNCA experiments were performed at 600 MHz. The following were used for the resonance assignment of the module pairs (37°C, 600 MHz unless stated otherwise): ^{1}H,^{15}N heteronuclear single-quantum coherence (HSQC) spectra (Mori et al., 1995) and 3D experiments HNCACB, CBCA(CO)NH (Muhandiram and Kay, 1994), HNCO (Kay et al., 1994), HN(CA)CO (Engelke and Ruterjans, 1995), HCC(CO)NH-TOCSY (Grzesiek and Bax, 1992; Logan et al., 1993), $HCCH_3$-TOCSY (Uhrín et al., 2000), (HB)CB(CGCDCE)HE, and (HB)CB(CGCD)HD (Yamazaki et al., 1993). A total correlation spectroscopy experiment (HCCH-TOCSY) (Kay et al., 1993) and ^{15}N- and ^{13}C-edited NOESYs (Pascal et al., 1994) were collected for each sample. In both cases, the ^{15}N-NOESY data were collected on the ^{15}N-labeled sample. The ^{13}C-NOESY spectra were collected on a 800 MHz spectrometer.

Slowly exchanging amide protons ($<1.0\ s^{-1}$) were identified by analysis of 2D heteronuclear water-exchange experiments (Mori et al., 1997). Partners for slowly exchanging protons were identified based on well-determined initial structures, supporting NOE data, and by consideration of the likely geometry of the putative H bond. Donor hydrogen-acceptor angles were constrained by appropriate distance restraints (Nilges et al., 1997). A semiconstant time HMSQC (Aitio and Permi, 2000) experiment was used to derive $^{3}J_{HN\text{-}HA}$ values. The raw NMR data were processed within AZARA (http://www.bio.cam.ac.uk/azara/).

Resonance Assignment—Structure Calculation

Spectra were viewed and atoms were assigned within ANSIG (Kraulis, 1989). Completely resolved ^{15}N-NOESY and ^{13}C-NOESY crosspeaks were picked and assigned unambiguously wherever possible. The "connect" program within AZARA converted normalized peak intensities into four distance categories of <2.7 Å, 3.3 Å, 5 Å, and 6 Å. Two separate lists, one of unambiguous NOE restraints, the other of ambiguous restraints (with possibilities generated from tables of δs), were thus produced by connect, allowing 0.03 ppm and 0.3 ppm margins of error in the ^{1}H and $^{15}N/^{13}C$ dimensions, respectively. These restraint files, along with the H bond and dihedral angle information, were input into CNS-based protocols and subjected to a simulated annealing protocol. Four "filtering" steps were performed on the ambiguous NOE list—the first three steps eliminating assignment possibilities that contributed <1% to the total NOE, and the final one eliminating residues that contributed <2%. In all, 120 structures were calculated for each module pair, and 24 selected on the basis of having lowest NOE-derived energies.

Reconstruction of CR1∼15–17 was based on the experimentally determined structures of CR1∼15,16 and CR1∼16,17 and performed using Modeller v. 4 (Sali and Blundell, 1993). Module 16 of CR1∼15–17 was modeled on CR1∼15,16 *and* CR1∼16,17, except for residues (always in loops) where rmsds were >0.6 Å. In these cases, if the loop was nearer (in space) to CCP 15, then $^{(15)}16$ was used as the template, while if the loop was proximal to CCP 17, $16^{(17)}$ was used to derive the model. This method aimed to preserve the character of the experimentally determined module-module junctions. The standard homology modeling method was used (Sali and Blundell, 1993) to calculate 100 models of CR1∼15–17, with the adjustment of the van der Waals radii scaling factor from the default of 0.82 to 1.00. The models are obtained by optimization of a molecular probability function using a variable target function in Cartesian space that employs methods of conjugate gradients and molecular dynamics with simulated annealing.

Relaxation Studies

^{15}N T_1 and T_2 relaxation times were measured by the method of Kay et al. (1992) with water flip-back pulses inserted when the magnetization was in the HzNz state; the τ_{cp} delay in the CPMG part of the T_2 sequence was 0.9 ms. Soft pulse WATERGATE was used for water suppression (Piotto et al., 1992). The heteronuclear ^{1}H-^{15}N steady-state NOEs were recorded keeping the water along the *z* axis. For measurements of T_1 in CR1∼15,16, delays of 12.2, 12.2, 55.8, 110.3, 219.3, 328.3, 546.3, and 818.8 ms were used; delays of 16.6, 16.6, 32.51, 48.77, 65.02, 97.54, 130.05, and 162.56 ms were used for T_2 measurements. To measure T_1 in CR1∼16,17, delays of 12.2, 12.2, 110.3, 415.5, 546.3, 753.4, 873.3, and 960.5 ms were used; delays of 16.6, 16.6, 48.19, 64.26, 80.32, 96.38, 96.38, and 112.45 ms were utilized for measurement of T_2. For both proteins a reference ^{1}H-^{15}N NOE experiment was recorded with 5 s relaxation delay. A second ^{1}H-^{15}N NOE spectrum was recorded with saturation of ^{1}H achieved by a train of ^{1}H 120° pulses applied for the last 3 s of the 5 s delay. Spectra were processed within AZARA and assigned according to ^{15}N,^{1}H δs of relevant HSQC spectra using ANSIG. A single exponential decay was fitted to the extracted peak heights for each residue to obtain the relaxation rates using nonlinear fitting.

Residual Dipolar Couplings

^{15}N-^{1}H RDCs were measured for a 0.3 mM sample of ^{15}N-labeled CR1∼15,16 in 2% cetylpyridinium bromide/hexanol with a residual ^{2}H splitting of ∼3.1 Hz and for a similar, nonaligned sample using an IPAP pulse sequence (Ottiger et al., 1998). A total of 94 residual dipolar couplings (RDCs) were extracted. The RDCs of residues considered to be mobile (low ^{1}H,^{15}N NOE or in slow exchange) were then eliminated, leaving 55 RDCs (25 in CCP 15, 30 in CCP 16) as input for subsequent calculations. Magnitudes and orientations of the alignment tensors were calculated for CCPs 15 and 16 independently from each of the structures in the ensemble (Losonczi et al., 1999).

Constructs for Functional Assays

Mutations were made using QuikChange™ site-directed mutagenesis kit (Stratagene, La Jolla, CA). A modified LHR C (i.e., modules 15–21) (Krych et al., 1994) with site 2 identical to that used in NMR studies (no N glycosylation sites at N918 and N987) was used as a template for mutagenesis. Plasmid pSG5 (Stratagene) containing cDNA for LHR C or its derivatives was transfected into 293T human kidney cells (Smith et al., 2000) using LipofectAMINE (Life Technologies, Inc.) as described (Krych-Goldberg et al., 1999). Binding and cofactor assays were performed as described (Krych et al., 1994).

Acknowledgments

Work in St. Louis was supported by CytoMed and by National Institutes of Health grant R01 A141592 to J.P.A. Work in Edinburgh was supported by the Wellcome Trust, Biotechnology and Biological Sciences Research Council (BBSRC), Darwin Trust (K.B.), and Edinburgh Protein Interaction Centre. We thank Dr. Que Van for implementing TROSY-based sequences and Dr. Dani Nietlispath (Cambridge National High-Field NMR Facillity) for expert assistance with the 800 MHz spectrometer.

Received: October 22, 2001
Revised: February 8, 2002

References

Aitio, H., and Permi, P. (2000). Semi-constant-time HMSQC (SCT-HMSQC-HA) for the measurement of (3)J(HNH alpha) couplings in N-15-labeled proteins. J. Magn. Reson. *143*, 391–396.

Barbato, G., Ikura, M., Kay, L.E., Pastor, R.W., and Bax, A.Y. (1992). Backbone dynamics of calmodulin studied by ^{15}N relaxation using inverse detected two dimensional NMR spectroscopy: the central helix is flexible. Biochemistry *31*, 5269–5278.

Barlow, P.N., Steinkasserer, A., Norman, D.G., Kieffer, B., Wiles, A.P., Sim, R.B., and Campbell, I.D. (1993). Solution structure of a pair of complement modules by nuclear magnetic resonance. J. Mol. Biol. *232*, 268–284.

Blom, A.M., Zadura, A.F., Villoutreix, B.O., and Dahlback, B. (2000). Positively charged amino acids at the interface between alpha-chain CCP1 and CCP2 of C4BP are required for regulation of the classical C3-convertase. Mol. Immunol. *37*, 445–453.

Bork, P., Downing, A.K., Kieffer, B., and Campbell, I.D. (1996). Structure and distribution of modules in extracellular proteins. Q. Rev. Biophys. *29*, 119–167.

Bouma, B., De Groot, P.G., Van Den Elsen, J.M.H., Ravelli, R.B.G., Schouten, A., Simmelink, M.J., Derksen, R.H.W.M., Kroon, J., and Gros, P. (1999). Adhesion mechanism of human β2-glycoprotein I to phospholipids based on its crystal structure. EMBO J. *18*, 5166–5173.

Casasnovas, J.M., Larvie, M., and Stehle, T. (1999). Crystal structure of two CD46 domains reveals an extended measles virus-binding surface. EMBO J. *18*, 2911–2922.

Clark, N.S., Dodd, I., Mossakowska, D.E., Smith, R.A., and Gore, M.G. (1996). Folding and conformational studies on SCR 1–3 domains of human complement receptor 1. Protein Eng. *9*, 877–884.

Cole, J.L., Housley, G.A., Jr., Dykman, T.R., MacDermott, R.P., and Atkinson, J.P. (1985). Identification of an additional class of C3-binding membrane proteins of human peripheral blood leukocytes and cell lines. Proc. Natl. Acad. Sci. USA *82*, 859–863.

Copie, V., Tomita, Y., Akiyama, S.K., Aota, S., Yamada, K.M., Venable, R.M., Pastor, R.W., Krueger, S., and Torchia, D.A. (1998). Solution structure and dynamics of linked cell attachment modules of mouse fibronectin containing the RGD and synergy regions: comparison with the human fibronectin crystal structure. J. Mol. Biol. *277*, 663–682.

Engelke, J., and Ruterjans, H. (1995). Sequential protein backbone resonance assignments using an improved 3D-HN(CA)CO pulse scheme. J. Magn. Reson. B *109*, 318–322.

Grzesiek, S., and Bax, A. (1992). Improved 3D triple-resonance NMR techniques applied to a 31-kDa protein. J. Magn. Reson. *96*, 432–440.

Henderson, C.E., Bromek, K., Mullin, N.P., Smith, B.O., Uhrin, D., and Barlow, P.N. (2001). Solution structure and dynamics of the central CCP module pair of a poxvirus complement control protein. J. Mol. Biol. *307*, 323–339.

Hourcade, D., Miesner, D.R., Atkinson, J.P., and Holers, V.M. (1988). Identification of an alternative polyadenylation site in the human C3b/C4b receptor (complement receptor type 1) transcriptional unit and prediction of a secreted form of complement receptor type 1. J. Exp. Med. *168*, 1255–1270.

Hutchinson, E.G., and Thornton, J.M. (1996). PROMOTIF—a program to identify and analyze structural motifs in proteins. Protein Sci. *5*, 212–220.

Kay, L.E., Nicholson, L.K., Delaglio, F., Bax, A., and Torchia, D.A. (1992). Pulse sequences for removal of effects of cross correlation between dipolar and chemical shift anisotropy relaxation mechanisms on the measurement of heteronuclear T_1 and T_2 values in proteins. J. Magn. Reson. *97*, 359–375.

Kay, L.E., Xu, G.Y., Singer, A.U., Muhandiram, D.R., and Forman-Kay, J.D. (1993). A gradient-enhanced HCCH-TOCSY experiment for recording side-chain H-1 and C-13 correlations in H_2O samples of proteins. J. Magn. Reson. B *101*, 333–337.

Kay, L.E., Xu, G.Y., and Yamazaki, T. (1994). Enhanced-sensitivity triple-resonance spectroscopy with minimal H_2O saturation. J. Magn. Reson. A *109*, 129–133.

Kirkitadze, M.D., and Barlow, P.N. (2001). Structure and flexibility of the multiple domain proteins that regulate complement activation. Immunol. Rev. *180*, 146–161.

Kirkitadze, M., Krych, M., Uhrin, D., Dryden, D., Cooper, A., Wang, X., Hauhart, R., Atkinson, J.P., and Barlow, P.N. (1999a). Independently melting modules and highly structured intermodular junctions within complement receptor type 1. Biochemistry *38*, 7019–7031.

Kirkitadze, M.D., Dryden, D.T.F., Kelly, S.M., Price, N.C., Wang, X., Krych, M., Atkinson, J.P., and Barlow, P.N. (1999b). Co-operativity between modules within a C3b-binding site of complement receptor type 1. FEBS Lett. *459*, 133–138.

Kirkitadze, M., Jumel, K., Harding, S., Dryden, D., Krych, M., Atkinson, J.P., and Barlow, P.N. (1999c). Combining ultracentrifugation with fluorescence to follow the unfolding of modules 16–17 of complement receptor type 1. Prog. Colloid Polym Sci. *113*, 164–167.

Klickstein, L.B., Wong, W.W., Smith, J.A., Weis, J.H., Wilson, J.G., and Fearon, D.T. (1987). Human C3b/C4b receptor (CR1). Demonstration of long homologous repeating domains that are composed of the short consensus repeats characteristics of C3/C4 binding proteins. J. Exp. Med. *165*, 1095–1112.

Klickstein, L.B., Bartow, T.J., Miletic, V., Rabson, L.D., Smith, J.A., and Fearon, D.T. (1988). Identification of distinct C3b and C4b recognition sites in the human C3b/C4b receptor (CR1, CD35) by deletion mutagenesis. J. Exp. Med. *168*, 1699–1717.

Kraulis, P.J. (1989). ANSIG: a program for the assignment of protein ^{1}H 2D NMR spectra by interactive graphics. J. Magn. Reson. *24*, 627–633.

Kraulis, P.J. (1991). MOLSCRIPT: a program to produce both detailed and schematic plots of protein structures. J. Appl. Crystallogr. *24*, 9446–9950.

Krych, M., Hourcade, D., and Atkinson, J.P. (1991). Sites within the complement C3b/C4b receptor important for the specificity of ligand binding. Proc. Natl. Acad. Sci. USA *88*, 4353–4357.

Krych, M., Clemenza, L., Howdeshell, D., Hauhart, R., Hourcade, D., and Atkinson, J.P. (1994). Analysis of the functional domains of complement receptor type 1 (C3b/C4b receptor, CD35) by substitution mutagenesis. J. Biol. Chem. *269*, 13273–13278.

Krych, M., Hauhart, R., and Atkinson, J.P. (1998). Structure-function analysis of the active sites of complement receptor type 1. J. Biol. Chem. *273*, 8623–8629.

Krych-Goldberg, M., and Atkinson, J.P. (2001). Structure-function relationships of complement receptor type 1. Immunol. Rev. *180*, 112–122.

Krych-Goldberg, M., Hauhart, R.E., Subramanian, B.Y., Yurcisin, B.M., II, Crimmins, D.L., Hourcade, D.E., and Atkinson, J.P. (1999). Decay accelerating activity of complement receptor type 1 (CD35). J. Biol. Chem. *274*, 31160–31168.

Kuttner-Kondo, L., Medof, M.E., Brodbeck, W., and Shoham, M. (1996). Molecular modeling and mechanism of action of human decay-accelerating factor. Protein Eng. *9*, 1143–1149.

Kuttner-Kondo, L.A., Mitchell, L., Hourcade, D.E., and Medof, M.E. (2001). Characterization of the active sites in decay-accelerating factor. J. Immunol. *167*, 2164–2171.

Liszewski, M.K., and Atkinson, J.P. (1998). Regulatory proteins of complement. In The Human Complement System in Health and Disease, J.E. Volanakis and M.M. Franks, eds. (New York: Marcel Dekker), pp. 149–166.

Liszewski, M.K., Leung, M., Cui, W., Subramanian, V.B., Parkinson, J., Barlow, P.N., Manchester, M., and Atkinson, J.P. (2000). Dissecting sites important for complement regulatory activity in membrane cofactor protein (MCP; CD46). J. Biol. Chem. *275*, 37692–37701.

Logan, T.M., Olejniczak, E.T., Xu, R.X., and Fesik, S.W. (1993). A general-method for assigning NMR-spectra of denatured proteins using 3D HC(CO)NH-TOCSY resonance experiments. J. Biomol. NMR *3*, 225–231.

Losonczi, J.A., Andrec, M., Fischer, M.W., and Prestegard, J.H. (1999). Order matrix analysis of residual dipolar couplings using singular value decomposition. J. Magn. Reson. *138*, 334–342.

Mori, S., Abeygunawardana, C., Johnson, M.O., and van Zijl, P.C.M. (1995). Improved sensitivity of HSQC spectra of exchanging protons at short interscan delays using a new fast HSQC (FHSQC) detection scheme that avoids water saturation. J. Magn. Reson. B *108*, 94–98.

Mori, S., Abeygunawardana, C., Berg, J.M., and van Zijl, P.C.M. (1997). NMR study of rapidly exchanging backbone amide protons in staphylococcal nuclease and the correlation with structural and dynamic properties. J. Am. Chem. Soc. *119*, 6844–6852.

Muhandiram, D.R., and Kay, L.E. (1994). Gradient enhanced triple resonance three-dimensional NMR experiments with improved sensitivity. J. Magn. Reson. B *103*, 203–216.

Murthy, K.H., Smith, S.A., Ganesh, V.K., Judge, K.W., Mullin, N., Barlow, P.N., Ogata, C.M., and Kotwal, G.J. (2001). Crystal structure of a complement control protein that regulates both pathways of complement activation and binds heparan sulfate proteoglycans. Cell *104*, 301–311.

Nelson, R.A., Jr. (1953). The immune adherence phenomenon. Science *118*, 733–737.

Nelson, D.S. (1963). Immune adherence. Adv. Immunol. *3*, 131.

Nilges, M., Macias, M.J., O'Donoghue, S.I., and Oschkinat, H. (1997). Automated NOESY interpretation with ambiguous distance re-

straints: the refined NMR solution structure of the pleckstrin homology domain from beta-spectrin. J. Mol. Biol. *269*, 408–422.

Oran, A.E., and Isenman, D.E. (1999). Identification of residues within the 727–767 segment of human complement component C3 important for its interaction with factor H and with complement receptor 1 (CR1, CD35). J. Biol. Chem. *274*, 5120–5130.

Ottiger, M., Delaglio, F., and Bax, A. (1998). Measurement of J and dipolar couplings from simplified two-dimensional NMR spectra. J. Magn. Reson. *131*, 373–378.

Pascal, S.M., Muhandiram, D.R., Yamazaki, T., Forman-Kay, J.D., and Kay, L.E. (1994). Simultaneous acquisition of N-15-edited and C-13-edited NOE spectra of proteins dissolved in H_2O. J. Magn. Reson. B *103*, 197–201.

Piotto, M., Saudek, V., and Sklenar, V. (1992). Gradient-tailored excitation for single-quantum NMR-spectroscopy of aqeous solutions. J. Biomol. NMR *2*, 661–665.

Reid, K.B.M., and Day, A.J. (1988). Structure-function relationships of the complement components. Immunol. Today *10*, 177–180.

Reilly, B.D., and Mold, C. (1997). Quantitative analysis of C4Ab and C4Bb binding to the C3b/C4b receptor (CR1, CD35). Clin. Exp. Immunol. *110*, 310–316.

Rowe, J.A., Moulds, J.M., Newbold, C.I., and Miller, L.H. (1997). *P. falciparum* rosetting mediated by a parasite-variant erythrocyte membrane protein and complement-receptor 1. Nature *388*, 292–295.

Rowe, J.A., Rogerson, S.J., Raza, A., Moulds, J.M., Kazatchkine, M.D., March, K., Newbold, C.I., Atkinson, J.P., and Miller, L.H. (2000). Mapping of the region of complement receptor (CR) 1 required for *Plasmodium falciparum* rosetting and demonstration of the importance of CR1 in rosetting in field isolates. J. Immunol. *165*, 6341–6346.

Sali, A., and Blundell, T. (1993). Comparative protein modelling by satisfaction of spatial restraints. J. Mol. Biol. *234*, 779–815.

Salzmann, M., Wider, G., Pervushin, K., Senn, H., and Wüthrich, K. (1999). TROSY-type triple-resonance experiments for sequential NMR assignments of large proteins. J. Am. Chem. Soc. *121*, 844–848.

Schwarzenbacher, R., Zeth, K., Diederichs, K., Gries, A., Kostner, G.M., Laggner, P., and Prassi, R. (1999). Crystal structure of human β2-glycoprotein I: implications for phospholipid binding and the antiphospholipid syndrome. EMBO J. *18*, 6228–6239.

Smith, H.R., Chuang, H.H., Wang, L.L., Salcedo, M., Heusel, J.W., and Yokoyama, W.M. (2000). Nonstochastic coexpression of activation receptors on murine natural killer cells. J. Exp. Med. *191*, 1341–1354.

Subramanian, V.B., Clemenza, L., Krych, M., and Atkinson, J.P. (1996). Substitution of two amino acids confers C3b binding to the C4 binding site of CR1 (CD35). J. Immunol. *157*, 1242–1247.

Szakonyi, G., Guthridge, J.M., Li, D., Young, K., Holers, M., and Chen, X.S. (2001). Structure of Complement Receptor 2 in complex with its C3d ligand. Science *292*, 1725–1728.

Uhrín, D., Uhrínová, S., Leadbeater, C., Nairn, J., Price, N.C., and Barlow, P.N. (2000). 3D $HCCH_3$-TOCSY for resonance assignment of methyl-containing side chains in C-13-labeled proteins (2000). J. Magn. Reson. *142*, 288–293.

Villoutreix, B.O., Hardig, Y., Wallqvist, A., Covell, D.G., Garcia de Frutos, P., and Dahlback, B. (1998). Structural investigation of C4b-binding protein by molecular modeling: localization of putative binding sites. Proteins *31*, 391–405.

Weisman, H.F., Bartow, T., Leppo, M.K., Marsh, H.C., Jr., Carson, G.R., Concino, M.F., Boyle, M.P., Roux, K.H., Weisfeldt, M.L., and Fearon, D.T. (1990). Soluble human complement receptor type 1: in vivo inhibitor of complement suppressing post-ischemic myocardial inflammation and necrosis. Science *249*, 146–151.

Wiles, A.P., Shaw, G., Bright, J., Perczel, A., Campbell, I.D., and Barlow, P.N. (1997). NMR studies of a viral protein that mimics the regulators of complement activation. J. Mol. Biol. *272*, 253–265.

Wong, W.W., and Farrell, S.A. (1991). Proposed structure of the F' allotype of human CR1. Loss of a C3b binding site may be associated with altered function. J. Immunol. *146*, 656–662.

Yamazaki, T., Forman-Kay, J.D., and Kay, L.E. (1993). Two-dimensional NMR experiments for correlating C-13-beta and H-1-delta/epsilon chemical-shifts of aromatic residues in C-13-labeled proteins via scalar couplings. J. Am. Chem. Soc. *115*, 11054–11055.

Accession Numbers

Coordinates of CR1∼15,16 (1gkn), CR1∼16,17 (1gkg), and the reconstructed structure of CR1∼15–17 (1gop) have been deposited at the Protein Data Bank.